Performance Analysis of Uplink/Downlink Decoupled Access in Cellular-V2X Networks

Luofang Jiao , *Member, IEEE*, Kai Yu , *Member, IEEE*, Jiacheng Chen , *Member, IEEE*, Tingting Liu , *Member, IEEE*, Haibo Zhou , *Senior Member, IEEE*, and Lin Cai , *Fellow, IEEE*

Abstract—This paper first develops an analytical framework to investigate the performance of uplink (UL)/downlink (DL) decoupled access in cellular vehicle-to-everything (C-V2X) networks, in which a vehicle's UL/DL can be connected to different macro/small base stations (MBSs/SBSs), separately. Using the stochastic geometry analytical tool, the UL/DL decoupled access C-V2X is modeled as a Cox process, and we obtain the following theoretical results, i.e., 1) the probability of different UL/DL joint association cases i.e., both the UL and DL are associated with the different MBSs or SBSs, or they are associated with different types of BSs; 2) the distance distribution of a vehicle to its serving BSs in each case; 3) the spectral efficiency of UL/DL in each case; and 4) the UL/DL coverage probability of MBS/SBS. The analyses reveal the insights and performance gain of UL/DL decoupled access. Through extensive simulations, the accuracy of the proposed analytical framework is validated. Both the analytical and simulation results show that UL/DL decoupled access can improve spectral efficiency. The theoretical results can be directly used for estimating the statistical performance of a UL/DL decoupled access C-V2X network.

Index Terms—C-V2X, uplink/downlink decoupled access, association probability, spectral efficiency, stochastic geometry.

I. INTRODUCTION

A. Background and Motivation

CELLULAR vehicle-to-everything (C-V2X) is vital for autonomous driving and intelligent transportation systems

(ITS) in the fifth-generation mobile networks (5G) and beyond [1], [2], [3], [4]. To satisfy the stringent quality-of-service (QoS) requirements of various C-V2X applications [5], [6], small base stations (SBS) can be deployed alongside the macro base stations (MBS) [7]. Decoupled access of uplink (UL) and downlink (DL) is a promising technology and its performance has been investigated in typical cellular networks [8], [9]. In decoupled access networks, a user equipment (UE) is allowed to simultaneously connect with an MBS and an SBS for separate UL/DL transmission [10], so both UL and DL can utilize the most appropriate BSs.

Given the increased spectrum frequency and the heightened demands of vehicular users' services, the C-V2X is gradually evolving into a more complicated heterogeneous network including MBSs and SBSs [8], [11], [12]. The traditional DL receiving power-based UL association mode is already not appropriate for C-V2X. In this paper, we study the UL/DL decoupled access C-V2X networks to provide an in-depth understanding of decoupled access in C-V2X through theoretical analysis and to investigate its potential performance gain in terms of spectral efficiency (SE). The major challenge comes from the complexity of distributions of roads, vehicles, SBSs and MBSs [12], [13]. Specifically, in C-V2X networks, vehicles and SBSs are randomly distributed along the roads following a Poisson point process (PPP). The roads can be modeled as lines of a Poisson line process (PLP), and the roads and the MBSs are randomly distributed on a two-dimensional (2D) plane following a PLP and PPP, respectively [14]. In contrast, in typical cellular networks, both UEs and BSs are assumed independently distributed on a 2D plane following a PPP. Therefore, the traditional UL/DL decoupled analysis methods in cellular networks are not applicable in C-V2X.

B. Related Work

Recently, the UL/DL decoupled access has been shown to outperform traditional coupled access in cellular networks. For example, Zhang et al. theoretically investigated the UL performance improvement under the UL/DL decoupled mode over the coupled access mode in [15]. Li et al. studied the UL SE in multiuser multiple-input multiple-output (MIMO) heterogeneous networks and revealed the superiority of decoupled mode over coupled mode [16]. In [17], Smiljkovikj et al. first derived the probability of different cases of UL/DL decoupled association in heterogeneous wireless networks. A more recent work [18]

presented an in-depth analysis of SE in UL/DL decoupled cellular networks. In [19], Yu et al. proposed a novel fully-decoupled RAN (FD-RAN) architecture for 6G. Shi et al. proposed a decoupled access scheme with enhanced energy efficiency for cellular-enabled UAV communication networks [20]. Different from the works mentioned above, our analysis jointly considers UL and DL in the decoupled access C-V2X networks, in which distributions of roads, vehicles, SBSs, and MBSs are different types of Poisson processes and are independent.

C-V2X is a special application scenario of cellular networks with UEs, i.e., vehicles, moving fast along the roads. In [21], Pan et al. presented the coverage probability analysis for safety messages-prioritized C-V2X communications. In [22] and [23], Chetlur et al. presented DL coverage and rate analysis in C-V2X. Sial et al. introduced a tractable analytical framework for performance of C-V2X networks over shared V2V and cellular UL channels [24]. In [25], Liu et al. studied millimeter wave (mmWave) communications of UL by leveraging the stochastic geometry theory in C-V2X. Yu et al. introduced a reinforcement learning-based RAN slicing framework for V2X communications with the aid of UL/DL decoupled access [26]. It is demonstrated that this technology can significantly improve load balancing and reduce the transmit power. Despite the contributions of existing works on C-V2X, there still lacks a thorough performance analysis for the UL/DL decoupled access C-V2X networks.

C. Contributions

This paper fills the gap in the performance analysis of decoupled access in C-V2X networks. First, we use variants of the Poisson process to model the distributions of roads, vehicles, SBSs, and MBSs in the C-V2X. Note that vehicles and SBSs are actually modeled by the 'doubly stochastic' Cox process since they are distributed only alongside the roads. Then, stochastic geometry is adopted as the mathematical tool to obtain the following four key results, namely 1) the probabilities of four different UL/DL joint association cases (i.e., UL=DL=MBS/SBS, UL=MBS/SBS, and DL=SBS/MBS), given by Lemma 1–3; 2) distribution of vehicle's distance to its serving BSs, given by Lemma 4–6; 3) SE of UL/DL in all cases, given by Theorem 1–6; and 4) coverage probability (CP) of UL/DL of MBS/SBS, given by Theorem 7–10. Besides, SE of coupled access associated with MBS/SBS is given by Corollary 1 such that the performance of decoupled and coupled access can be compared in theory under the same analytical framework. To summarize, the contributions of this paper are listed as follows:

- We propose a tractable analytical framework for UL/DL decoupled access in C-V2X considering random distributions of roads, vehicles, SBSs, and MBSs.
- We provide theoretical results on UL/DL decoupled joint association probability, distance distributions for all decoupled cases, SE of all links and CP are given. The effect of speed is analyzed to study the mobility of vehicular networks. The theoretical results can be directly used for estimating the statistical performance of a UL/DL decoupled access C-V2X network.

TABLE I
LIST OF MAJOR SYMBOLS

Notation	Description
v, λ	The speed of vehicle. The density of vehicle and BS.
x^*	The location of closest BS to vehicle.
P	Received and transmit power of vehicle, SBS, and MBS.
G, g	The main lobe gain and side lobe gain.
H, χ	The channel gain and Nakagami-m fading gain.
$\Gamma(\cdot)$	The gamma distribution function of a random variable.
t	The predetermined threshold t of CP or SE.
Ξ_l	The Poisson line process of lines.
$\Xi_{l_i}^S, \Xi_{l_i}^V$	The Poisson point processes of vehicles and SBSs on line i.
Θ_V, Θ_S	The Cox processes of vehicles and SBSs.
I_i	Interference from set i.
$Pr(\cdot)$	The probability of a random variable.
$E(\cdot)$	The expectation of a random variable.
$F(\cdot)$	The cumulative distribution function of a random variable.
$f(\cdot)$	The probability density function of a random variable.
$\zeta_I(\cdot)$	Laplace transform of interference I.
$\mathbb{K}(\cdot; \cdot; \cdot; \cdot)$	The newly defined function for $\zeta_I(\cdot)$.
τ_i^n	The SE of n, $n \in \{DL, UL\}$ for Case i.

- We conduct extensive simulations to verify the accuracy of the proposed analytical framework, and the results show better performance in UL/DL decoupled C-V2X networks in terms of load balance and SE, which will shed light on the further study of UL/DL decoupled access in C-V2X.

The remainder of this paper is organized as follows. Section II introduces the network model. In Section III, the analysis of decoupled access in C-V2X is presented. The simulation results are given and discussed in Section IV. The paper is concluded in Section V.

II. SYSTEM MODEL

A. Modeling of C-V2X Network

We consider a two-tier heterogeneous UL/DL decoupled access C-V2X network, which consists of MBSs, SBSs, and vehicles. For the convenience of readers, the mathematical parameters used in this paper are summarized in Table I. The MBSs are randomly distributed on a 2D plane. We first model the spatial layout of MBSs by a 2D PPP Φ_M with density λ_m in the euclidean plane. The locus of points that are geometrically closer to the selected MBSs than to any other MBS form a Voronoi cell. Then we model the roads by a PLP Ξ_l with intensity λ_l [27]. Since the SBSs and vehicles are distributed along the roads, we model the locations of vehicles and SBSs on each line $L_i \in \Xi_l$ by 1D PPPs $\Xi_{l_i}^S$ and $\Xi_{l_i}^V$ with densities λ_s and λ_v, respectively. Both $\Xi_{l_i}^S$ and $\Xi_{l_i}^V$ follow 1D PPPs with constant densities. Therefore, the locations of vehicles and SBSs follow Cox processes $\Theta_V = \{\Xi_{l_i}^V\}_{\{l_i \in \Xi_l\}}$, $\Theta_S = \{\Xi_{l_i}^S\}_{\{l_i \in \Xi_l\}}$, respectively [14]. It is worth mentioning that the Cox processes Θ_V and Θ_S are stationary and this property will be used in calculating the intensity in Section II-B [28]. In C-V2X, the mobility of vehicles can affect the macroscopic traffic density [29].

For our study, we choose one vehicle as the typical node and translate it to the origin $o \equiv (0, 0)$. Since the typical vehicle must be located on a road, and the road must pass through the origin, we set this road as a typical road l_o. The roads that do not

pass through the origin are referred to as the other roads. Under Palm probability of vehicle point process, the vehicles and SBSs on the typical road form the point process $\Theta_{V_o} = \Theta_V \cup \Xi_{L_o}^V$ and $\Theta_{S_o} = \Theta_S \cup \Xi_{L_o}^S$. Both the processes Θ_{V_o} and Θ_{S_o} are the superposition of a Cox process Θ_i and an independent 1D PPP $\Xi_{L_o}^i$ on line L_o, where $i \in \{V, S\}$. The results are derived via the application of Slivnyak's theorem to the line process Ξ_l [22], [28].

B. Propagation Model

We assume that the MBSs transmit to vehicles on the typical road and the other roads with the same power. Since SBSs and vehicles mainly communicate with the nodes on the road where they are located, we assume that SBSs and vehicles use transmit beamforming to maximize the received power at the receivers. Due to the non-identical behavior of the individual transmit and receive chains of SBSs and vehicles, we assume non-reciprocity channels.

We assume that all the MBSs have the same transmitting power P_M. All the SBSs and the vehicles have the same transmit power P_S and P_V, respectively. Because the SBSs and vehicles use directional antennas [30], we assume a beam pattern whose main lobes are along the roads on which the nodes are located and the side lobes facing other directions. We use $G_{S,0}$, $G_{V,0}$ and $G_{S,1}$, $G_{V,1}$ to denote the main lobe gains and side lobe gains of SBSs and vehicles, respectively. Since the MBSs have a larger service range and are randomly arranged, we assume that the MBSs have omnidirectional antennas and use G_M to denote the gains of MBSs. The general Nakagami-m fading is chosen to model the wide-range fading environment [31]. We use m_M to denote the fading parameter for the links between the typical vehicle and MBSs (VM) and H_M to denote the channel fading gains for DL of VM. The SBSs on the typical road are more likely to have line-of-sight (LOS) links to the typical vehicle than to vehicles on the other roads. Therefore, we denote the UL/DL fading parameters between the SBSs and vehicles as $m_{S,0}$, $m_{V,0}$ on the typical road, and $m_{S,1}$ $m_{V,1}$ on the other roads. The $H_{S,0}$, $H_{S,1}$ denote the corresponding fading gains in DL for the links between the typical vehicle and SBSs on the typical road (VST), and the links between the typical vehicle and SBSs on the other roads (VSO), respectively. The $H_{V,0}$ and $H_{V,1}$ denote the corresponding fading gains in UL for the links of VST and VSO, respectively. The fading gains follow a Gamma distribution and its probability density function (PDF) is [32]

$$f_{H_i} = \frac{m_i^{m_i} h^{m_i-1}}{\Gamma(m_i)} e^{-m_i h}, i \in \{M, S, V\}. \tag{1}$$

For the wireless links, we consider a standard power-law path-loss model with the decay rate $\|d\|^{-\alpha}$, where d indicates the distance between the transmitter and receiver and α is used to denote the path-loss exponent [33]. Given the different size and deployment locations of MBS and SBS, the path loss exponents of vehicle-SBS and that of vehicle-MBS may be different, which are denoted by α_S, α_M, respectively. Furthermore, for the effects of shadowing, we need to consider the links VST, VSO, and VM.

Therefore, random variables $\chi_{S,0}$, $\chi_{S,1}$, and χ_M following a log-normal distribution given by $10log_{10}\chi_i \sim \aleph(\omega_i, \delta_i^2)$ [34], are used to denote the shadowing effect of VST, VSO, and VM links, respectively. Hence, the received signal power of the typical vehicle from SBSs on the typical road, SBSs on the other roads and MBSs in DL is [23]

$$P_{r,V} = \begin{cases} P_M G_M H_M \chi_M \|x\|^{-\alpha_M}, & x \in \Phi_M \\ P_S G_{S,0} H_{S,0} \chi_{S,0} \|x\|^{-\alpha_S}, & x \in \Xi_{l_0}^S \\ P_S G_{S,1} H_{S,1} \chi_{S,1} \|x\|^{-\alpha_S}, & x \in \Theta_S \backslash \Xi_{l_0}^S. \end{cases} \tag{2}$$

Similarly, the received signal power in UL can be written as

$$P_{r,M} = P_V G_{V,1} H_{V,1} \chi_M \|x\|^{-\alpha_M}, \quad x \in \Theta_V , \tag{3}$$

$$P_{r,S} = \begin{cases} P_V G_{V,0} H_{V,0} \chi_{S,0} \|x\|^{-\alpha_S}, & x \in \Xi_{l_0}^V \\ P_V G_{V,1} H_{V,1} \chi_{S,1} \|x\|^{-\alpha_S}, & x \in \Theta_V \backslash \Xi_{l_0}^V, \end{cases} \tag{4}$$

where the $P_{r,V}$, $P_{r,M}$ and $P_{r,S}$ are the received signal power of the typical vehicle, MBS and SBS, respectively.

Modeling the channel with shadow fading causes the received power to not be exponentially distributed [35]. To cope with this issue, we refer to the lemma of displacement theorem in [36] and express it as a random displacement of the location of a typical receiver [37]. Thus, $P_r(x) = PG\chi\|x\|^{-\alpha}$ can be written as $P_r(y) = PG\|y\|^{-\alpha}$, where $y = \chi^{-\frac{1}{\alpha}}x$, and then the transformed points form a 2D homogeneous PPP with intensity λ to $E[\chi^{-\frac{2}{\alpha}}]\lambda$, and the 1D PPP's intensity is λ to $E[\chi^{-\frac{1}{\alpha}}]\lambda$. Therefore, the transformaed $\lambda_M = E[\chi_M^{-\frac{2}{\alpha}}]\lambda_m$, $\lambda_S = E[\chi_{S,0}^{-\frac{2}{\alpha}}]\lambda_m$, $\lambda_V = E[\chi_{S,0}^{-\frac{1}{\alpha}}]\lambda_m$. In $\Theta_S \backslash \Xi_{l_0}^S$ and $\Theta_V \backslash \Xi_{l_0}^V$, using the Theorem 1 and Assumption 1 in [23], the vehicles and SBSs can be asymptotically converged to 2D PPPs with intensity $\lambda_{Sa} = E[\chi_{S,1}^{-\frac{2}{\alpha}}]\pi\lambda_l\lambda_s$ and $\lambda_{Va} = E[\chi_{S,1}^{-\frac{2}{\alpha}}]\pi\lambda_l\lambda_v$, respectively. We use Φ_M^t, Θ_S^t, $\Xi_{l_0}^{S,t}$, Θ_V^t, $\Xi_{l_0}^{V,t}$ to denote the set for MBSs, SBSs, SBSs on the typical road, vheicles, vehicles on the typical road after executing the random displacement, respectively. Hence, the value of $P_{r,V}$, $P_{r,M}$, and $P_{r,S}$ after undergoing random replacement can be obtained through similar procedures as the above steps.

C. Association Policy for BSs and Vehicles

UL/DL decoupled access C-V2X allow vehicles to choose to access different BSs for UL and DL, separately [8]. As shown in Fig. 1, the four cases of joint UL/DL association in decoupled access C-V2X networks are:

- Case 1: UL = MBS 1, DL = MBS 2
- Case 2: UL = SBS, DL = MBS
- Case 3: UL = MBS, DL = SBS
- Case 4: UL = SBS 1, DL = SBS 2

However, there are only two cases for the coupled access, i.e., UL/DL = MBS and UL/DL = SBS. It is noticed that the decoupled access's Case 1 and Case 4 are connected to two BSs instead of the same BS, while the coupled access's UL depends on DL and both the UL and DL access the same BS. We assume that the typical vehicle is associated with MBS/SBS which yields the maximum received power (MRP) in DL. Similarly, the MBS/SBS will serve the vehicle with the MRP in UL. Thus,

the typical vehicle associates with an MBS in DL if

$$P_M G_M x_M^{-\alpha_M} > P_S G_{S,0} x_S^{-\alpha_S}, \quad (5)$$

where x_M, x_S denotes the nearest distances that the corresponding MBS $\in \Phi_M^t$ and SBS $\in \Xi_{l_0}^{S,t}$ to the typical vehicle. Otherwise, the vehicle connects to an SBS. Similarly, the typical vehicle associates with an MBS in UL if and only if

$$P_V G_{V,1} x_M^{-\alpha_M} > P_V G_{V,0} x_S^{-\alpha_S}. \quad (6)$$

Otherwise, the typical vehicle associates with an SBS. We substitute (5) and (6) with $A_{M,S} = P_M G_M / P_S G_{S,0}$, $B_{M,S} = P_V G_{V,1} / P_V G_{V,0}$:

$$A_{M,S} x_M^{-\alpha_M} > x_S^{-\alpha_S}, \quad (7)$$

$$B_{M,S} x_M^{-\alpha_M} > x_S^{-\alpha_S}, \quad (8)$$

Since the transmit power of MBS is much larger than that of the SBS and vehicle, thus, $A_{M,S}$ is larger than $B_{M,S}$. Meanwhile, the association based on MRP is then equal to that based on the minimum distance, i.e., each vehicle will communicate with the closest BS after executing the procedure of random displacement.

D. Interference

Different frequencies are used for UL and DL, there is no interference between DL and UL. The transmission signal of MBS and SBS is interfered by the signals transmitted from the other BSs, and the typical vehicle's interference comes from other vehicles.

Because all SBSs and MBSs use the same frequency for DL and all vehicles use another frequency for UL, in DL [38], the aggregate interference of the typical vehicle is composed of the interference from the MBSs I_M, the interference from the SBSs on the typical road $I_{S,0}$ and the interference from the SBSs on other roads $I_{S,1}$. In UL, the aggregate interference is composed of the interference from the vehicles on the typical roads $I_{V,0}$ and the interference from the vehicles on the other roads $I_{V,1}$. Thus, when the typical vehicle is associated with MBS or SBS in DL, the measured signal-to-noise-and-interference-ratio (SINR) is

$$SINR_{M/S,D} = \frac{P(X_d^*)}{I_M + I_{S,0} + I_{S,1} + \sigma_D^2}, \quad (9)$$

where

$$I_M = \sum_{x \in \Phi_M} P_M G_M H_M \|x\|^{-\alpha_M};$$

$$\Phi = \begin{cases} \Phi_M^t \backslash X_d^*, & DL = MBS, d = M \\ \Phi_M^t, & DL = SBS, \end{cases} \quad (10)$$

$$I_{S,0} = \sum_{x \in \Xi} P_S G_{S,0} H_{S,0} \|x\|^{-\alpha_S};$$

$$\Xi = \begin{cases} \Xi_{l_0}^{S,t}, & DL = MBS, \\ \Xi_{l_0}^{S,t} \backslash X_d^*, & DL = SBS, d = S, 0, \end{cases} \quad (11)$$

$$I_{S,1} = \sum_{x \in \Theta_S^t \backslash \Xi_{l_0}^{S,t}} P_S G_{S,1} H_{S,1} \|x\|^{-\alpha_S}. \quad (12)$$
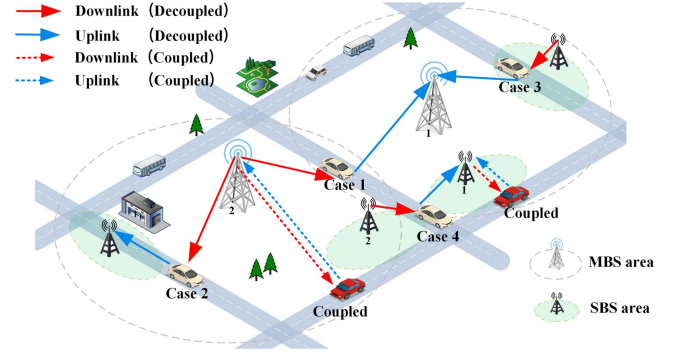

Fig. 1. Illustration of UL/DL decoupled access in C-V2X networks.

Here, the X_d^* is the distance between the typical vehicle and the associated BS. When the typical vehicle connects to the MBS or SBS, the $d = M, d = S, 0$, respectively. $\Phi_M^t \backslash X_M^*$ denotes that the interference I_M is from the MBSs except for the connected MBS when $DL = MBS$. $\Xi_{l_0}^{S,t} \backslash X_{S,0}^*$ denotes that the interference $I_{S,0}$ is from the SBSs except for the connected SBS when $DL = SBS$. The SINR measured in UL is

$$SINR_{M/S,U} = \frac{P(X^*)}{I_{V,0} + I_{V,1} + \sigma_U^2}, \quad (13)$$

where

$$I_{V,0} = \sum_{x \in \Xi_{l_0}^{V,t} \backslash X^*} P_V G_{V,q} H_{V,q} \|x\|^{-\alpha_k},$$

$$\{k, q\} = \begin{cases} DL=MBS : k = M, q = 1 \\ DL=SBS : k = S, q = 0. \end{cases} \quad (14)$$

$$I_{S,1} = \sum_{x \in \Theta_V^t \backslash \Xi_{l_0}^{V,t}} P_V G_{V,1} H_{V,1} \|x\|^{-\alpha_k}. \quad (15)$$

Here, since the vehicles use directional antenna and the MBSs are not along the road, when the vehicle accesses an MBS in UL, the $\alpha_k = \alpha_M, G_{V,q} = G_{V,1}$, when the vehicle accesses a SBS in UL, the $\alpha_k = \alpha_S, G_{V,q} = G_{V,0}$. Since the noise is much smaller than the interference and the system is interference limited, the thermal noise can be neglected for the sake of convenient analysis, therefore, $\sigma_U^2 = \sigma_D^2 = 0$ [18], [23].

III. PERFORMANCE ANALYSIS AND THEORETICAL RESULTS

With the help of stochastic geometry, we first derive the association probabilities and the distributions of distance for all UL/DL joint association cases. Then, based on the above results, the SE of each UL/DL link in each case, and the CP of UL/DL for MBS/SBS are derived.

A. Association Probability

According to the null probability of 1D and 2D PPP [39], the cumulative distribution functions (CDF) of x_S, x_M are

$$F_S(x_S) = 1 - \exp(-2\lambda_S x_S), \quad (16)$$

$$F_M(x_M) = 1 - \exp(-\lambda_M \pi x_M^2). \quad (17)$$

Hence, the PDFs of x_S, x_M are

$$f_S(x_S) = 2\lambda_S \exp(-2\lambda_S x_S), \tag{18}$$

$$f_M(x_M) = 2\pi x_M \lambda_M \exp(-\lambda_M \pi x_M^2). \tag{19}$$

According to the association policy given by (7) and (8), we derive the joint association probability as follows:

1) Case 1 (UL = MBS 1, DL = MBS 2): The probability that the typical vehicle is associated to MBS both in DL and UL is

$$\Pr(Case\,1) = \Pr\left(A_{M,S} X_M^{-\alpha_M} > X_S^{-\alpha_S};\right.$$

$$\left. B_{M,S} X_M^{-\alpha_M} > X_S^{-\alpha_S}\right). \tag{20}$$

Based on the consideration of $A_{M,S} > B_{M,S}$, the above formula can be written as

$$\Pr(Case\,1) = \Pr\left(B_{M,S} X_M^{-\alpha_M} > X_S^{-\alpha_S}\right)$$

$$= \Pr\left(X_M < B_{M,S}^{\frac{1}{\alpha_M}} X_S^{\frac{\alpha_S}{\alpha_M}}\right). \tag{21}$$

Lemma 1: The joint association probability of Case 1 can be formulated as

$$\Pr(Case\,1)$$

$$= 1 - \int_0^\infty \left[2\lambda_S \exp\left(-\lambda_M \pi B_{M,S}^{\frac{2}{\alpha_M}} x_S^{\frac{2\alpha_S}{\alpha_M}} - 2\lambda_S x_S\right)\right] dx_S. \tag{22}$$

When $\alpha_S = \alpha_M$, Pr(Case 1) in closed form can be formulated as

$$\Pr(Case\,1) =$$

$$1 - \sqrt{\frac{\lambda_S^2}{\lambda_M B_{M,S}^{\frac{2}{\alpha}}}} \exp\left(\frac{\lambda_S^2}{\lambda_M \pi B_{M,S}^{\frac{2}{\alpha}}}\right) erfc\left(\frac{\lambda_S}{\sqrt{\lambda_M \pi B_{M,S}^{\frac{2}{\alpha}}}}\right). \tag{23}$$

Proof: The proof of joint association probability of Case 1 (UL = MBS 1, DL = MBS 2) is

$$\Pr(Case\,1)$$

$$= Pr(B_{M,S} X_M^{-\alpha_M} > X_S^{-\alpha_S})$$

$$= E_{X_S}\left[\Pr\left(X_M < B_{M,S}^{\frac{1}{\alpha_M}} x_S^{\frac{\alpha_S}{\alpha_M}} | X_S\right)\right]$$

$$= \int_0^\infty F_M\left(B_{M,S}^{\frac{1}{\alpha_M}} x_S^{\frac{\alpha_S}{\alpha_M}}\right) f_S(x_S) dx_S$$

$$\overset{(a)}{=} 1 - \int_0^\infty \left[2\lambda_S \exp\left(-\lambda_M \pi B_{M,S}^{\frac{2}{\alpha_M}} x_S^{\frac{2\alpha_S}{\alpha_M}} - 2\lambda_S x_S\right)\right] dx_S, \tag{24}$$

where (a) follows from the substituting $F_M(\cdot)$ and $f_S(\cdot)$ from (17) and (18) in the previous steps. ∎

2) Case 2 (UL = SBS, DL = MBS): The probability that the typical vehicle is associated to MBS in DL and SBS in UL is

$$\Pr(Case\,2)$$

$$= \Pr\left(A_{M,S} X_M^{-\alpha_M} > X_S^{-\alpha_S}; B_{M,S} X_M^{-\alpha_M} < X_S^{-\alpha_S}\right)$$

$$= \Pr\left(B_{M,S} X_M^{-\alpha_M} < X_S^{-\alpha_S} < A_{M,S} X_M^{-\alpha_M}\right). \tag{25}$$

Lemma 2: The joint association probability of Case 2 can be formulated as

$$\Pr(Case\,2)$$

$$= \int_0^\infty \left[2\lambda_S \exp\left(-\lambda_M \pi B_{M,S}^{\frac{2}{\alpha_M}} x_S^{\frac{2\alpha_S}{\alpha_M}} - 2\lambda_S x_S\right)\right] dx_S$$

$$- \int_0^\infty \left[2\lambda_S \exp\left(-\lambda_M \pi A_{M,S}^{\frac{2}{\alpha_M}} x_S^{\frac{2\alpha_S}{\alpha_M}} - 2\lambda_S x_S\right)\right] dx_S. \tag{26}$$

When $\alpha_S = \alpha_M$, Pr(Case 2) in closed form is:

$$\Pr(Case\,2) =$$

$$\sqrt{\frac{\lambda_S^2}{\lambda_M B_{M,S}^{\frac{2}{\alpha}}}} \exp\left(\frac{\lambda_S^2}{\lambda_M \pi B_{M,S}^{\frac{2}{\alpha}}}\right) erfc\left(\frac{\lambda_S}{\sqrt{\lambda_M \pi B_{M,S}^{\frac{2}{\alpha}}}}\right)$$

$$- \sqrt{\frac{\lambda_S^2}{\lambda_M A_{M,S}^{\frac{2}{\alpha}}}} \exp\left(\frac{\lambda_S^2}{\lambda_M \pi A_{M,S}^{\frac{2}{\alpha}}}\right) erfc\left(\frac{\lambda_S}{\sqrt{\lambda_M \pi A_{M,S}^{\frac{2}{\alpha}}}}\right). \tag{27}$$

Proof: The proof of joint association probability of Case 2 (UL = SBS, DL = MBS) is

$$\Pr(Case\,2)$$

$$\overset{(a)}{=} \Pr\left(X_M < A_{M,S}^{\frac{1}{\alpha_M}} X_S^{\frac{\alpha_S}{\alpha_M}}\right)$$

$$- \Pr\left(X_M < B_{M,S}^{\frac{1}{\alpha_M}} X_S^{\frac{\alpha_S}{\alpha_M}}\right)$$

$$\overset{(b)}{=} E_{X_S}\left[\Pr\left(X_M < A_{M,S}^{\frac{1}{\alpha_M}} x_S^{\frac{\alpha_S}{\alpha_M}} | X_S\right)\right]$$

$$- E_{X_S}\left[\Pr\left(X_M < B_{M,S}^{\frac{1}{\alpha_M}} x_S^{\frac{\alpha_S}{\alpha_M}} | X_S\right)\right]$$

$$= \int_0^\infty F_M\left(A_{M,S}^{\frac{1}{\alpha_M}} x_S^{\frac{\alpha_S}{\alpha_M}}\right) f_S(x_S) dx_S$$

$$- \int_0^\infty F_M\left(B_{M,S}^{\frac{1}{\alpha_M}} x_S^{\frac{\alpha_S}{\alpha_M}}\right) f_S(x_S) dx_S$$

$$= \int_0^\infty \left[2\lambda_S \exp\left(-\lambda_M \pi B_{M,S}^{\frac{2}{\alpha_M}} x_S^{\frac{2\alpha_S}{\alpha_M}} - 2\lambda_S x_S\right)\right] dx_S$$

$$- \int_0^\infty \left[2\lambda_S \exp\left(-\lambda_M \pi A_{M,S}^{\frac{2}{\alpha_M}} x_S^{\frac{2\alpha_S}{\alpha_M}} - 2\lambda_S x_S\right)\right] dx_S, \tag{28}$$

where Pr(Case 2) can be converted to (a). Then in (b), the result is converted to derive the expectations for X_s. The remaining derivations are similar in Lemma 1. ∎

3) Case 3 (UL = MBS, DL = SBS): The probability that the typical vehicle is associated to MBS in UL and SBS in DL is

$$\Pr\left(Case\,3\right) = \Pr\left(A_{M,S}X_M^{-\alpha_M} < X_S^{-\alpha_S};\right.$$
$$\left.B_{M,S}X_M^{-\alpha_M} > X_S^{-\alpha_S}\right), \qquad (29)$$

Since $A_{M,S}$ is larger than $B_{M,S}$, there is no region that satisfies (29). Hence, $\Pr(Case\,3) = 0$.

4) Case 4 (UL = SBS 1, DL = SBS 2): The probability that the typical vehicle is associated to SBS both in UL and DL is:

$$\Pr\left(Case\,4\right) = \Pr\left(A_{M,S}X_M^{-\alpha_M} < X_S^{-\alpha_S};\right.$$
$$\left.B_{M,S}X_M^{-\alpha_M} < X_S^{-\alpha_S}\right)$$
$$= \Pr\left(A_{M,S}X_M^{-\alpha_M} < X_S^{-\alpha_S}\right)$$
$$= \Pr\left(X_S < A_{S,M}^{\frac{1}{\alpha_S}}X_M^{\frac{\alpha_M}{\alpha_S}}\right). \qquad (30)$$

Lemma 3: The joint association probability of Case 4 can be formulated as

$$\Pr\left(Case\,4\right)$$
$$= \int_0^\infty \left[2\lambda_S \exp\left(-\lambda_M\pi A_{M,S}^{\frac{2}{\alpha_M}}x_S^{\frac{2\alpha_S}{\alpha_M}} - 2\lambda_S x_S\right)\right]dx_S, \qquad (31)$$

When $\alpha_S = \alpha_M$, $\Pr(Case\,4)$ in closed form is

$$\Pr\left(Case\,4\right)$$
$$= \sqrt{\frac{\lambda_S^2}{\lambda_M A_{M,S}^{\frac{2}{\alpha}}}}\exp\left(\frac{\lambda_S^2}{\lambda_M\pi A_{M,S}^{\frac{2}{\alpha}}}\right)erfc\left(\frac{\lambda_S}{\sqrt{\lambda_M\pi A_{M,S}^{\frac{2}{\alpha}}}}\right). \qquad (32)$$

Proof: The proof of joint association probability of Case 4 (UL = SBS 1, DL = SBS 2) is

$$\Pr(Case\,4)$$
$$= \Pr\left(X_S^{-\alpha_S} > A_{M,S}X_M^{-\alpha_M}\right)$$
$$\overset{(a)}{=} 1 - \Pr(X_M < A_{M,S}^{\frac{1}{\alpha_M}}X_S^{\frac{\alpha_S}{\alpha_M}})$$

$$\overset{(b)}{=} \int_0^\infty \left[2\lambda_S \exp\left(-\lambda_M\pi A_{M,S}^{\frac{2}{\alpha_M}}x_S^{\frac{2\alpha_S}{\alpha_M}} - 2\lambda_S x_S\right)\right]dx_S, \qquad (33)$$

where because the original form is hard to derive, we change to calculate the probability of its complement in (a). (b) can be derived by following the steps as adopted in Lemma 1. ∎

B. Distribution of Distance to BSs

In this subsection, we derive the distance distributions of typical vehicle to its serving BSs for all feasible cases.

Lemma 4: The distance distribution of Case 1 is

$$f_{X_M|Case\,1} = \frac{\exp\left(-\lambda_S\pi 2B_{S,M}^{\frac{1}{\alpha_S}}x^{\frac{\alpha_M}{\alpha_S}}\right)f_{X_M}(x)}{\Pr\left(Case\,1\right)}. \qquad (34)$$

Proof: To derive the distance distribution of Case 1, we need to compute the CCDF as

$$F_{X_M|Case\,1}^C$$
$$= \Pr\left(X_M > x \,\Big|\, B_{M,S}X_M^{-\alpha_M} > X_S^{-\alpha_S}\right)$$
$$= \frac{\Pr\left(X_M > x; B_{M,S}X_M^{-\alpha_M} > X_S^{-\alpha_S}\right)}{\Pr\left(Case\,1\right)}$$
$$= \frac{\Pr(X_M > x; X_S > B_{S,M}^{\frac{1}{\alpha_S}}X_M^{\frac{\alpha_M}{\alpha_S}})}{\Pr\left(Case\,1\right)}$$
$$= \frac{\int_x^\infty \left[\exp\left(-\lambda_S\pi 2B_{S,M}^{\frac{1}{\alpha_S}}x_M^{\frac{\alpha_M}{\alpha_S}}\right)f_{X_M}(x_M)\right]dx_M}{\Pr\left(Case\,1\right)}, \qquad (35)$$

then the CDF is $F_{X_M|Case\,1} = 1 - F_{X_M|Case\,1}^C$. At last, we can achieve the PDF by differentiating CDF: $f_{X_M|Case\,1} = dF_{X_M|Case\,1}/dx$.

Similarly, the proofs of Lemmas 4, 5, and 6 can be derived by following the steps as adopted here. ∎

Lemma 5: The distance distributions of Case 2 are formulated as given in (36) and (37) shown at the bottom of this page.

Proof: Similar to the proof of Lemma 4. ∎

Lemma 6: The distance distribution of Case 4 is formulated as

$$f_{X_S|Case\,4} = \frac{\exp\left(-\lambda_M\pi A_{M,S}^{\frac{2}{\alpha_M}}x^{\frac{2\alpha_S}{\alpha_M}}\right)f_{X_S}(x)}{\Pr\left(Case\,4\right)}. \qquad (38)$$

$$f_{X_M|Case\,2} = \frac{\left[\exp\left(-\lambda_S\pi 2A_{S,M}^{\frac{1}{\alpha_S}}x^{\frac{\alpha_M}{\alpha_S}}\right) - \exp\left(-\lambda_S\pi 2B_{S,M}^{\frac{1}{\alpha_S}}x^{\frac{\alpha_M}{\alpha_S}}\right)\right]f_{X_M}(x)}{\Pr\left(Case\,2\right)}, \qquad (36)$$

$$f_{X_S|Case\,2} = \frac{\left[\exp\left(-\lambda_M\pi B_{M,S}^{\frac{2}{\alpha_M}}x^{\frac{\alpha_S}{\alpha_M}}\right) - \exp\left(-\lambda_M\pi A_{M,S}^{\frac{2}{\alpha_M}}x^{\frac{\alpha_S}{\alpha_M}}\right)\right]f_{X_S}(x)}{\Pr\left(Case\,2\right)}. \qquad (37)$$

Proof: Similar to the proof of Lemma 4. ■

C. Spectral Efficiency

SE refers to the amount of data transmitted per unit of bandwidth. In this subsection, with results of Lemma 1 to 6, we derive the SE of each case by leveraging stochastic geometry [40].

The average system SE is

$$SE = \sum_{i=1}^{4} \sum_{L}^{\{U,D\}} \tau_{Case\ i}^{L} Pr\left(Case\ i\right), \quad (39)$$

where τ_i is the average SE of Case i.

To make the statement clearer, we first derive the SE of UL for Case 2.

Theorem 1: The SE of UL for Case 2 is formulated as

$$\tau_2^U = \int_0^\infty f_{S|2} \int_0^\infty \Pr\left[H_{V,0} > \beta_{S,0} I_{U,2} x_S^{\alpha_S}\right] dt dx_S, \quad (40)$$

where $\beta_{S,0} = (e^t - 1)/(P_V G_{V,0})$, $I_{U,2} = I_{V,0} + I_{V,1}$. The $\Pr[H_{V,0} > \beta_{S,0} I_{U,2} x_S^{\alpha_S}]$ is

$$\Pr\left[H_{V,0} > \beta_{S,0} I_{U,2} x_S^{\alpha_S}\right]$$
$$= \sum_{k=0}^{m_S-1} \frac{(-m_S \beta_{S,0} x_S^{\alpha_S})^k}{k!} \left[\frac{\delta^k}{\delta j^k} \zeta_{I_{U,2}}(j)\right]_{j=m_S \beta_{S,0} x_S^{\alpha_S}}, \quad (41)$$

where $\zeta_{I_{U,2}}(j) = \zeta_{I_{V,0}}(j)\zeta_{I_{V,1}}(j)$,

$$\zeta_{I_{S,0}}(j) = \mathbb{K}\left(\lambda_V; x_s; \frac{P_V G_{V,0} x^{-\alpha_S}}{m_S}; m_S; 1\right), \quad (42)$$

$$\zeta_{I_{S,1}}(j) = \mathbb{K}\left(\pi \lambda_{Va}; 0; \frac{P_V G_{V,1} x^{-\alpha_S}}{m_{S,1}}; m_{S,1}; x\right). \quad (43)$$

Proof: The SE of Case 2 UL is

$$\tau_2^U = E\left[\ln\left(1 + SINR_{U,S}\right)\right]$$
$$= \int_0^\infty f_{S|2} \int_0^\infty \Pr\left[\ln\left(1 + \frac{P_V G_{V,0} H_{V,0} x_S^{-\alpha_S}}{I_{U,2}}\right) > t\right] dt dx_S$$
$$= \int_0^\infty f_{S|2} \int_0^\infty \Pr\left[H_{V,0} > \frac{(e^t - 1) I_{U,2}}{P_V G_{V,0}} x_S^{\alpha_S}\right] dt dx_S$$
$$\overset{(a)}{=} \int_0^\infty f_{S|2} \int_0^\infty \Pr\left[H_{V,0} > \beta_{S,0} I_{U,2} x_S^{\alpha_S}\right] dt dx_S, \quad (44)$$

where $\beta_{S,0} = (e^t - 1)/(P_V G_{V,0})$ in (a). The proof of $\Pr[H_{V,0} > \beta_{S,0} I_{U,2} x_S^{\alpha_S}]$ is

$$\Pr\left[H_{V,0} > \beta_{S,0} I_{U,2} x_S^{\alpha_S}\right]$$
$$= E_{I_S}\left\{\Pr\left[H_{V,0} > \beta_{S,0} I_{U,2} x_S^{\alpha_S}\right]\right\}$$
$$\overset{(a)}{=} E_{I_S}\left[\frac{\Gamma\left(m_S, m_S \beta_{S,0} I_{U,2} x_S^{\alpha_S}\right)}{\Gamma\left(m_S\right)}\right]$$
$$\overset{(b)}{=} E_{I_S}\left[\sum_{k=0}^{m_S-1} \frac{(m_S \beta_{S,0} I_{U,2} x_S^{\alpha_S})^k}{k!} e^{-m_S \beta_{S,0} I_S x_S^{\alpha_S}}\right]$$
$$= \sum_{k=0}^{m_S-1} \frac{(-m_S \beta_{S,0} x_S^{\alpha_S})^k}{k!} \left[\frac{\delta^k}{\delta j^k} \zeta_{I_{U,2}}(j)\right]_{j=m_S \beta_{S,0} x_S^{\alpha_S}}, \quad (45)$$

where (a) follows from the CCDF of gamma random variable $H_{V,0}$, and (b) follows from the definition of incomplete gamma function for integer values of m_S. The aggregate interference can be divided into two independent components $I_{V,0}, I_{V,1}$, the Laplace transform of interference can be computed as product of the Laplace transforms of the two components, thus, $\zeta_{I_{U,2}}(j) = \zeta_{I_{V,0}}(j)\zeta_{I_{V,1}}(j)$. Similar to the proof of Lemma 5 in [23], the Laplace transforms of $I_{V,0}$ and $I_{V,1}$ are

$$\zeta_{I_{V,0}}(j)$$
$$= E_{I_{V,0}}\left[\exp\left(-j I_{V,0}\right)\right]$$
$$= E_{I_{V,0}}\left[\exp\left(-j \sum_{x_S \in \Xi_{l_0}^{V,t} \setminus [-x_S, x_S]} P_V G_{V,0} H_{V,0} x^{-\alpha_S}\right)\right]$$
$$\overset{(a)}{=} E_{\Xi_{l_0}^{V,t} \setminus X^*} E_{H_{V,0}}\left[\prod_{x_S \in \Xi_{l_0}^{V,t} \setminus [-x_S, x_S]} e^{-j P_V G_{V,0} H_{V,0} x^{-\alpha_S}}\right]$$
$$\overset{(b)}{=} \exp\left[-2\lambda_V \int_{x_S}^\infty \left(1 - \left(1 + \frac{j P_V G_{V,0} x^{-\alpha_S}}{m_S}\right)^{-m_S}\right) dx\right]$$
$$\overset{(c)}{=} \mathbb{K}\left(\lambda_V; x_s; \frac{P_V G_{V,0} x^{-\alpha_S}}{m_S}; m_S; 1\right), \quad (46)$$

where (a) follows from the independence of $\Xi_{l_0}^{V,t}$, we convert the accumulative form into accumulative multiplication. (b) follows from the Nakagami-m fading assumption and the PGFL of a 1D PPP [41]. The proofs above are typical steps of stochastic geometry. We define a function $\mathbb{K}(a; b, c; d; e)$ to simplify (b) in (c), where a is the term before the integral except the constant, b is the lower limit of integration and the upper limit is always ∞, c is the fractional term in the integral except j, d is the index term, $e \in \{x, 1\}$ is the last integral term (x if there is, or 1 if not).

$$\zeta_{I_{V,1}}(j)$$
$$= E_{I_{V,1}}\left[\exp\left(-j I_{V,1}\right)\right]$$
$$= E_{I_{V,1}}\left[\exp\left(-j \sum_{x \in \Phi_V^t \setminus \Xi_{l_0}^{V,t}} P_V G_{V,1} H_{V,1} x^{-\alpha_S}\right)\right]$$
$$= E_{\Theta_S^t \setminus \Xi_{l_0}^{V,t}} E_{H_{V,1}}\left[\prod_{x \in \Theta_V^t \setminus \Xi_{l_0}^{V,t}} e^{-j P_V G_{V,1} H_{S,1} x^{-\alpha_S}}\right]$$
$$\overset{(a)}{=} \exp\left[-2\pi \lambda_{Va} \int_0^\infty 1 - \left(1 + \frac{j P_V G_{V,1} x^{-\alpha_S}}{m_{S,1}}\right)^{-m_{S,1}} x dx\right]$$
$$= \mathbb{K}\left(\pi \lambda_{Va}; 0; \frac{P_V G_{V,1} x^{-\alpha_S}}{m_{S,1}}; m_{S,1}; x\right), \quad (47)$$

where (a) follows from the PGFL of a 2D PPP. ■

Theorem 2: The SE of DL for Case 2 is formulated as

$$\tau_2^D = \int_0^\infty f_{M|2} \int_0^\infty \Pr\left[H_M > \beta_M I_{D,2} x_M^{\alpha_M}\right] dt dx_M, \quad (48)$$

where $\beta_M = (e^t - 1)/(P_M G_M)$, $I_{D,2} = I_M + I_{S,0} + I_{S,1}$. The $\Pr[H_M > \beta_M I_{D,2} x_M^{\alpha_M}]$ is

$$\Pr[H_M > \beta_M I_{D,2} x_M^{\alpha_M}]$$
$$= \sum_{k=0}^{m_M-1} \frac{(-m_M \beta_M x_M^{\alpha_M})^k}{k!} \left[\frac{\delta^k}{\delta j^k} \zeta_{I_{D,2}}(j) \right]_{j=m_M \beta_M x_M^{\alpha_M}}, \tag{49}$$

where the $\zeta_{I_{D,2}}(j) = \zeta_{I_M}(j)\zeta_{I_{S,0}}(j)\zeta_{I_{S,1}}(j)$. The $\Pr[H_M > \beta_M I_{D,1} x_M^{\alpha_M}]$ are

$$\zeta_{I_M}(j) = \mathbb{K}\left(\pi \lambda_M; x_M; \frac{P_M G_M x^{-\alpha_M}}{m_M}; m_M; x \right), \tag{50}$$

$$\zeta_{I_{S,0}}(j) = \mathbb{K}\left(\lambda_S; A_{S,M}^{\frac{1}{\alpha_S}} x_M^{\frac{\alpha_M}{\alpha_S}}; \frac{P_S G_{S,0} x^{-\alpha_S}}{m_{S,0}}; m_{S,0}; 1 \right), \tag{51}$$

$$\zeta_{I_{S,1}}(j) = \mathbb{K}\left(\pi \lambda_{Sa}; 0; \frac{P_V G_{S,1} x^{-\alpha_S}}{m_{S,1}}; m_{S,1}; x \right). \tag{52}$$

Proof: Follows by the same arguments as in the proof of Theorem 1. ∎

Theorem 3: The SE of UL for Case 1 is formulated as

$$\tau_1^U = \int_0^\infty f_{M|1} \int_0^\infty \Pr[H_{V,1} > \beta_M I_{U,1} x_M^{\alpha_M}] dt dx_M, \tag{53}$$

where $\beta_M = (e^t - 1)/(P_V G_{V,1})$, $I_{U,1} = I_{V,0} + I_{V,1}$. For the convenience of writing, we use $f_{M|1}(\cdot)$ to substitute $f_{X_M|Case 1}(\cdot)$ and the following PDFs reduce to the same form. And the $\Pr[H_M > \beta_M I_{U,1} x_M^{\alpha_M}]$ in τ_1^U is

$$\Pr[H_M > \beta_M I_{U,1} x_M^{\alpha_M}]$$
$$= \sum_{k=0}^{m_M-1} \frac{(-m_M \beta_M x_M^{\alpha_M})^k}{k!} \left[\frac{\delta^k}{\delta j^k} \zeta_{I_{U,1}}(j) \right]_{j=m_M \beta_M x_M^{\alpha_M}}, \tag{54}$$

where $\zeta_{I_{U,1}}(j)$ is the Laplace transform of $I_{U,1}$. From stochastic geometry, the accumulation becomes a multiplication relationship that greatly simplifies the calculation. Thus, $\zeta_{I_{U,1}}(j) = \zeta_{I_{V,0}}(j)\zeta_{I_{V,1}}(j)$. The $\zeta_{I_{V,0}}(j)$ and $\zeta_{I_{V,1}}(j)$ are

$$\zeta_{I_{V,0}}(j) = \mathbb{K}\left(\lambda_V; x_M; \frac{P_V G_{V,1} x^{-\alpha_M}}{m_M}; m_M; 1 \right), \tag{55}$$

$$\zeta_{I_{V,1}}(j) = \mathbb{K}\left(\pi \lambda_{Va}; 0; \frac{P_V G_{V,1} x^{-\alpha_M}}{m_M}; m_M; x \right). \tag{56}$$

Proof: The proof of Theorem 3 is similar to the proof of Case 2 in Theorem 1. ∎

Theorem 4: The SE of DL for Case 1 is formulated as

$$\tau_1^D = \int_0^\infty f_{M|1} \int_0^\infty \Pr[H_M > \beta_M I_{D,1} x_M^{\alpha_M}] dt dx_M, \tag{57}$$

where $\beta_M = (e^t - 1)/P_M G_M$, $I_{D,1} = I_M + I_{S,0} + I_{S,1}$. The $\Pr[H_M > \beta_M I_{D,1} x_M^{\alpha_M}]$ are

$$\Pr[H_M > \beta_M I_{D,1} x_M^{\alpha_M}]$$

$$= \sum_{k=0}^{m_M-1} \frac{(-m_M \beta_M x_M^{\alpha_M})^k}{k!} \left[\frac{\delta^k}{\delta j^k} \zeta_{I_{D,1}}(j) \right]_{j=m_M \beta_M x_M^{\alpha_M}}, \tag{58}$$

where the $\zeta_{I_M}(j) = \zeta_{I_M}(j)\zeta_{I_{S,0}}(j)\zeta_{I_{S,1}}(j)$, the $\zeta_{I_M}(j)$, $\zeta_{I_{S,0}}(j)$ and $\zeta_{I_{S,1}}(j)$ are

$$\zeta_{I_M}(j) = \mathbb{K}\left(\pi \lambda_M; x_M; \frac{P_M G_M x^{-\alpha_M}}{m_M}; m_M; x \right), \tag{59}$$

$$\zeta_{I_{S,0}}(j) = \mathbb{K}\left(\lambda_S; A_{S,M}^{\frac{1}{\alpha_S}} x_M^{\frac{\alpha_M}{\alpha_S}}; \frac{P_S G_{S,0} x^{-\alpha_S}}{m_{S,0}}; m_{S,0}; 1 \right), \tag{60}$$

$$\zeta_{I_{S,1}}(j) = \mathbb{K}\left(\pi \lambda_{Sa}; 0; \frac{P_S G_{S,1} x^{-\alpha_S}}{m_{S,1}}; m_{S,1}; x \right). \tag{61}$$

Proof: Follows by the same arguments as in the proof of Theorem 1. ∎

Theorem 5: The SE of UL for Case 4 is formulated as

$$\tau_4^U = \int_0^\infty f_{S|4} \int_0^\infty \Pr[H_{V,0} > \beta_S I_{U,4} x_S^{\alpha_S}] dt dx_S, \tag{62}$$

where $\beta_S = (e^t - 1)/(P_V G_{V,0})$, $I_{U,4} = I_{V,0} + I_{V,1}$. The $\Pr[H_S > \beta_S I_{U,4} x_S^{\alpha_S}]$ is

$$\Pr[H_S > \beta_S I_{U,4} x_S^{\alpha_S}]$$
$$= \sum_{k=0}^{m_S-1} \frac{(-m_S \beta_S x_S^{\alpha_S})^k}{k!} \left[\frac{\delta^k}{\delta j^k} \zeta_{I_{U,4}}(j) \right]_{j=m_S \beta_S x_S^{\alpha_S}}, \tag{63}$$

where $\zeta_{I_{U,4}}(j) = \zeta_{I_{V,0}}(j)\zeta_{I_{V,1}}(j)$, the $\zeta_{I_{V,0}}(j)$ and $\zeta_{I_{V,1}}(j)$ are the same as that in UL of Case 2.

Proof: The proof of Theorem 5 is similar to the proof of Case 2 in Theorem 1. ∎

Theorem 6: The SE of DL for Case 4 is formulated as

$$\tau_4^D = \int_0^\infty f_{S|4} \int_0^\infty \Pr[H_S > \beta_S I_{D,4} x_S^{\alpha_S}] dt dx_S, \tag{64}$$

where $\beta_S = (e^t - 1)/(P_S G_{S,0})$, $I_{D,4} = I_M + I_{S,0} + I_{S,1}$. The $\Pr[H_S > \beta_S I_{D,4} x_S^{\alpha_S}]$ is

$$\Pr[H_S > \beta_S I_{D,4} x_S^{\alpha_S}]$$
$$= \sum_{k=0}^{m_S-1} \frac{(-m_S \beta_S x_S^{\alpha_S})^k}{k!} \left[\frac{\delta^k}{\delta j^k} \zeta_{I_{D,4}}(j) \right]_{j=m_S \beta_S x_S^{\alpha_S}}, \tag{65}$$

where $\zeta_{I_{D,4}}(j) = \zeta_{I_M}(j)\zeta_{I_{S,0}}(j)\zeta_{I_{S,1}}(j)$. The Laplace transforms are

$$\zeta_{I_M}(j) = \mathbb{K}\left(\pi \lambda_M; 0; \frac{P_V G_M x^{-\alpha_M}}{m_M}; m_M; x \right), \tag{66}$$

$$\zeta_{I_{S,0}}(j) = \mathbb{K}\left(\lambda_S; x_S; \frac{P_S G_{S,0} x^{-\alpha_S}}{m_{S,0}}; m_{S,0}; 1 \right), \tag{67}$$

$$\mathcal{L}_{I_{S,1}}(j) = \mathbb{K}\left(\pi \lambda_{Sa}; 0; \frac{P_S G_{S,1} x^{-\alpha_S}}{m_{S,1}}; m_{S,1}; x \right). \tag{68}$$

Proof: The proof of Theorem 6 is similar to the proof of Case 2 in Theorem 1. ∎

Corollary 1: The coupled access has two association cases as shown in Fig. 1 and the SE of coupled access for the two association cases is similar to the SE of UL/DL decoupled access. The proof follows the same steps as in Theorem 1. Specifically, when the typical vehicle is associated with SBS, the case is equivalent to Case 4 of decoupled access [18]. Therefore, the SE of UL and DL in coupled access with SBS τ_S^U and τ_S^D are equal to τ_4^U and τ_4^D, respectively. When the typical vehicle connects to MBS, the SE of DL is

$$\tau_M^D = \int_0^\infty f_{M|MBS} \int_0^\infty \Pr\left[H_M > \beta_M I_{D,M} x_M^{\alpha_M}\right] dt dx_M, \tag{69}$$

where the $\beta_M = (e^t - 1)/(P_M G_M)$, and

$$\Pr\left[H_M > \beta_M I_{D,M} x_M^{\alpha_M}\right]$$
$$= \sum_{k=0}^{m_M-1} \frac{(-m_M \beta_M x_M^{\alpha_M})^k}{k!} \left[\frac{\delta^k}{\delta j^k} \zeta_{I_{D,M}}(j)\right]_{j=m_M\beta_M x_M^{\alpha_M}}, \tag{70}$$

$$f_{X_M|MBS} = \frac{\exp\left(-\lambda_S \pi 2 A_{S,M}^{\frac{1}{\alpha_S}} x^{\frac{\alpha_M}{\alpha_S}}\right) f_{X_M}(x)}{\Pr(M)}, \tag{71}$$

where

$$\Pr(M) = \Pr\left(A_{M,S} X_M^{-\alpha_M} > X_S^{-\alpha_S}\right)$$
$$= 1 - \Pr(Case\,4), \tag{72}$$

where $\Pr(Case\,4)$ is derived in Lemma 3. The $\zeta_{I_{D,M}}(j) = \zeta_{I_M}(j)\zeta_{I_{S,0}}(j)\zeta_{I_{S,1}}(j)$ and $\zeta_{I_M}(j)$, $\zeta_{I_{S,0}}(j)$, $\zeta_{I_{S,1}}(j)$ are the same with (50) to (52) in DL of Case 2.

The SE of UL is

$$\tau_M^U = \int_0^\infty f_{M|MBS} \int_0^\infty \Pr\left[H_M > \beta_M I_{U,M} x_M^{\alpha_M}\right] dt dx_M, \tag{73}$$

where $\beta_M = (e^t - 1)/(P_V G_V)$, and

$$\Pr\left[H_M > \beta_M I_{U,M} x_M^{\alpha_M}\right]$$
$$= \sum_{k=0}^{m_M-1} \frac{(-m_M \beta_M x_M^{\alpha_M})^k}{k!} \left[\frac{\delta^k}{\delta j^k} \zeta_{I_{U,M}}(j)\right]_{j=m_M\beta_M x_M^{\alpha_M}}. \tag{74}$$

The $\zeta_{I_{U,1}}(j) = \zeta_{I_{V,0}}(j)\zeta_{I_{V,1}}(j)$. And $\zeta_{I_{V,0}}(j)$, $\zeta_{I_{V,1}}(j)$ are equal to (55) and (56) in UL of Case 1.

D. Coverage Probability

The CP is defined as the probability that SINR exceeds a predetermined threshold t [42]. Based on the above results from (16) to (74), we derive the CP of UL/DL for MBS/SBS in this subsection.

Theorem 7: The CP of DL for MBS is

$$\Pr(SIR_D^M > t)$$
$$= P(Case\,1)P(SIR_D^M > t|1) + P(Case\,2)P(SIR_D^M > t|2)$$

$$= P(Case\,1) \sum_{k=0}^{m_M-1} \int_0^\infty \frac{(-m_M \beta_M x_M^{\alpha_M})^k}{k!} \times$$
$$\left[\frac{\delta^k}{\delta j^k} \zeta_{I_{D,M}}(j)\right]_j \times f_{M|1} dt + P(Case\,2)\times$$
$$\sum_{k=0}^{m_M-1} \int_0^\infty \frac{(-m_M \beta_M x_M^{\alpha_M})^k}{k!} \left[\frac{\delta^k}{\delta j^k} \zeta_{I_{D,M}}(j)\right] f_{M|2} dt, \tag{75}$$

where $j = m_M\beta_M x_M^{\alpha_M}$, $\beta_M = t/P_M G_M$. $\zeta_{I_{D,M}}(j) = \zeta_{I_M}(j)\zeta_{I_{S,0}}(j)\zeta_{I_{S,1}}(j)$ and the $\zeta_{I_{S,0}}(j)$, $\zeta_{I_{S,1}}(j)$ are the same with (59) to (61) in DL of Case 1.

Proof: The proof of Theorem 7 is similar to the proof of Case 2 in Theorem 1. ∎

Theorem 8: The CP of UL for MBS is

$$\Pr(SIR_U^M > t)$$
$$= P(Case\,1)P(SIR_U^M > t|1)$$
$$= P(Case\,1) \sum_{k=0}^{m_M-1} \int_0^\infty \frac{(-m_M \beta_M x_M^{\alpha_M})^k}{k!}$$
$$\left[\frac{\delta^k}{\delta j^k} \zeta_{I_{U,M}}(j)\right]_{j=m_M\beta_M x_M^{\alpha_M}} \times f_{M|1} dt, \tag{76}$$

where $j = m_M\beta_M x_M^{\alpha_M}$, $\beta_M = t/P_M G_M$. $\zeta_{I_{U,M}}(j) = \zeta_{I_{V,0}}(j)\zeta_{I_{V,1}}$ and the $\zeta_{I_{V,0}}(j)$, $\zeta_{I_{V,1}}(j)$ are the same with (55) to (56) in UL of Case 1.

Proof: The proof of Theorem 8 is similar to the proof of Case 2 in Theorem 1. ∎

Theorem 9: The CP of DL for SBS is

$$\Pr(SIR_D^S > t)$$
$$= P(Case\,4)P(SIR_D^S > t|1)$$
$$= P(Case\,4) \sum_{k=0}^{m_S-1} \int_0^\infty \frac{(-m_S \beta_S x_S^{\alpha_S})^k}{k!}$$
$$\left[\frac{\delta^k}{\delta j^k} \zeta_{I_{D,S}}(j)\right]_{j=m_S\beta_S x_S^{\alpha_S}} \times f_{S|4} dt, \tag{77}$$

where $\beta_S = t/P_S G_S$. $\zeta_{I_{D,S}}(j) = \zeta_{I_M}(j)\zeta_{I_{S,0}}(j)\zeta_{I_{S,1}}(j)$ and $\zeta_{I_M}(j)$, $\zeta_{I_{S,0}}(j)$, $\zeta_{I_{S,1}}(j)$ are the same with (66) to (68) in DL of Case 4.

Proof: The proof of Theorem 9 is similar to the proof of Case 2 in Theorem 1. ∎

Theorem 10: The CP of UL for SBS is

$$\Pr(SIR_U^S > t)$$
$$= P(Case\,2)P(SIR_U^S > t|2) + P(Case\,4)P(SIR_U^S > t|4)$$
$$= P(Case\,2) \sum_{k=0}^{m_S-1} \int_0^\infty \frac{(-m_S \beta_S x_S^{\alpha_S})^k}{k!}$$
$$\left[\frac{\delta^k}{\delta j^k} \zeta_{I_{U,S}}(j)\right]_{j=m_S\beta_S x_S^{\alpha_S}} \times f_{S|2} dt + P(Case\,4)$$

Simulation 1: Simulation for UL/DL Decoupled Access C-V2X.

Input: simulation number n, vehicle number V, SBS number s, MBS number m, road number L, simulation radius r, threshold t_τ, t_{CP}, maximum vehicle speed $v_{\max}$, maximum vehicle density $\lambda_{\max}$;

Output: Association probability $\mathbf{p} \in \mathbf{R}^{1\times 4}$, SE τ, CP;

1   Initialize $P \leftarrow \mathbf{0}_{n\times Vl}, \tau \leftarrow \mathbf{0}_{\mathbf{n}\times \mathbf{V}\mathbf{l}}, CP \leftarrow \mathbf{0}_{n\times Vl}, v$;
2   **for** $i = 1; i \leq n; i++$ **do**
3   Generate MBSs locations $\mathbf{m}$ follow PPP, road locations $\mathbf{l}$ follow PLP, SBSs locations $\mathbf{s}$ and vehicles locations $\mathbf{V}$ follow PPP on road l_i ;
4   **for** $l = 1; l \leq L; l++$ **do**
5   **for** $v = 1; v \leq V(l); v++$ **do**
6   According to (5) and (6), select Case $\mathbf{p}(i, v + \sum_{i=1}^{l-1} V(i)) = \{1, 2, 3, 4\}$;
7   Calculate SIR of UL/DL according (9);
8         $\tau(i, v + \sum_{i=1}^{l-1} V(i)) = \ln(1 + SIR)$, $\mathrm{CP}(i, v + \sum_{i=1}^{l-1} V(i)) = SIR$;
9   **end**
10   **end**
11    $p_o = \sum (p(i, :) == \{1, 2, 3, 4\})/\sum V)$;
12    $\tau_o = \sum (\tau(i, \mathrm{find}(\tau(i, :) > t_\tau)) > t_\tau)/(\sum V)$;
13    $CP_o = \sum (CP(i, :) > t_{CP})/(\sum V)$;
14   **end**
15   Return $p = \sum p_o/n$, $\tau = \sum \tau_o/n$, $CP = \sum CP_o/n$;

$$\sum_{k=0}^{m_S-1} \int_0^\infty \frac{(-m_S \beta_S x_S^{\alpha_S})^k}{k!} \left[\frac{\delta^k}{\delta j^k} \zeta_{I_{U,S}}(j) \right] \times f_{S|4} dt, \quad (78)$$

where $j = m_S \beta_S x_S^{\alpha_S}$, $\beta_S = t/P_V G_V$. $\zeta_{I_{U,S}}(j) = \zeta_{I_{V,0}}(j)\zeta_{I_{V,1}}(j)$ and the $\zeta_{I_{V,0}}(j)$, $\zeta_{I_{V,1}}(j)$ are the same with (55) to (56) in UL of Case 4.

Proof: The proof of Theorem 10 is similar to the proof of Case 2 in Theorem 1. ∎

IV. SIMULATION RESULTS

In this section, simulation results are presented. We consider a circular area of a 3 kilometers (km) radius with a two-tier network. The simulation setup follows 3GPP TR 36.885 [43] and the existing work [17], [22], [26], [44] and the values of parameters are listed in Table II. Over 100,000 independent Monte Carlo simulations are conducted in UL/DL decoupled access and coupled access scenarios, respectively, to validate the accuracy of the proposed analytical framework and theoretical results. The detailed steps of the simulation are in Simulation 1.

A. Joint Association Probabilities

In Fig. 2(a) and (b), the joint association probabilities from both analytical model and simulations for LOS and NLOS scenarios are shown. We can find that the analytical and simulation results match well, thereby demonstrating the accuracy of the proposed analytical model. Further, more details of joint UL/DL association in decoupled C-V2X can be obtained. In LOS scenario shown in Fig. 2(a), the typical vehicle chooses Case 2 with a

TABLE II
SYSTEM PARAMETERS

| Parameters	Value
Macro BS transmit power P_M (dBm)	46
Small BS transmit power P_S (dBm)	20
Vehicle transmit power P_V (dBm)	20
Pathloss exponent for MBS α_M	4
Pathloss exponent for SBS α_S (NLOS)	4
Pathloss exponent for SBS α_S (LOS)	2
Antenna Gain for MBS G_M (dBi)	0
Antenna Gain for vehicle in typical line G_{S0} (dBi)	0
Antenna Gain for vehicle in other line G_{S1} (dBi)	-20
Noise power $\sigma_D^2 = \sigma_U^2$	0
Maximum Speed $v_{\max}$ (km/h)	120
Maximum density of vehicle on road $\lambda_{\max}$ (nodes/km)	63
Line density λ_l (1/km)	10
Mean of log-normal shadowing gain (dB)	0
Std of shadowing gain for MBS (dB)	4
Std of shadowing gain for SBS on typical line (dB)	2
Std of shadowing gain for SBS on other lines (dB)	4
Nakagami-m $m_{S,0}$ (LOS/NLOS), $m_{S,1}$, m_M	{1,2}, 1, 1
Nakagami-m $m_{V,0}$ (LOS/NLOS), $m_{V,1}$	{1,2}, 1

(a) LOS

(b) NLOS
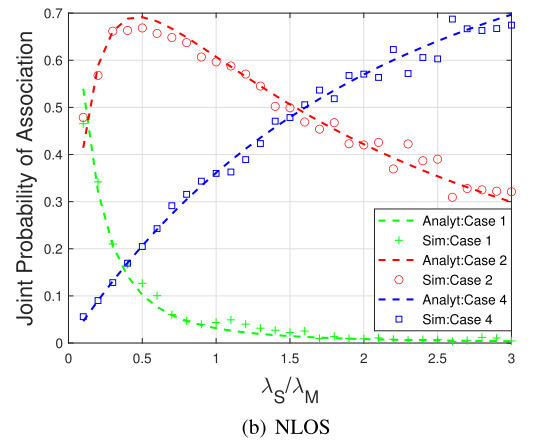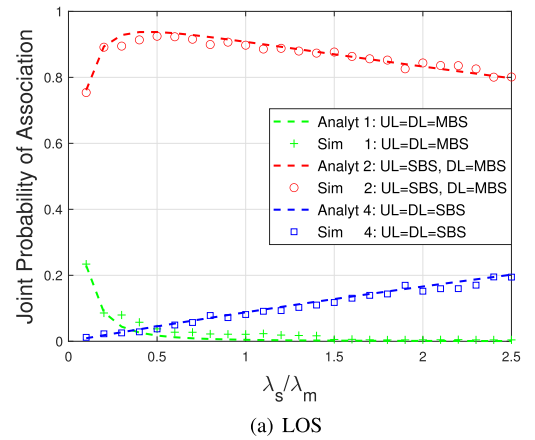
Fig. 2. Joint association probability of different cases in LOS and NLOS scenarios.

much higher probability. This is mainly because MBS has higher transmit power than SBS in DL, while in UL, the location of SBS is closer to the typical vehicle than MBS, so SBS has smaller signal path loss and larger antenna gain when receiving from the vehicle. In addition, since SBSs perform better than MBSs in UL, the probability of Case 1 decreases rapidly as there are more SBSs. The probability of Case 4 is gradually increasing with SBS density, since the distance between SBS and vehicle is

(a) $\lambda_s/\lambda_m = 2, \alpha_S = 3$

(b) $\lambda_s/\lambda_m = 4, \alpha_S = 3$

(c) $\lambda_s/\lambda_m = 2, \alpha_M = 3$

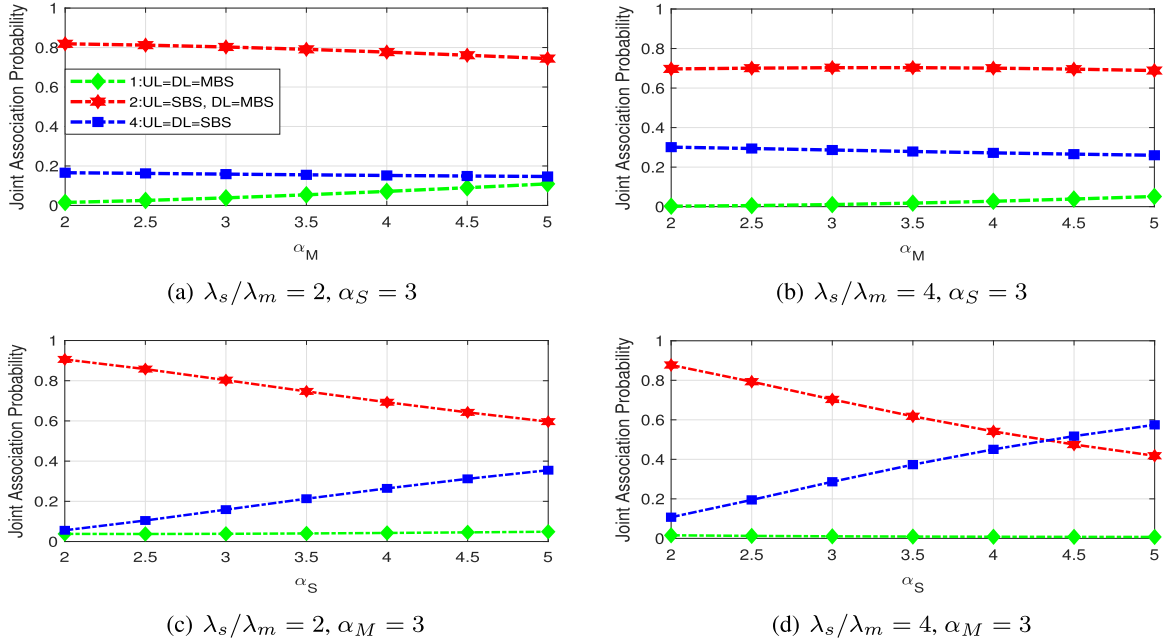(d) $\lambda_s/\lambda_m = 4, \alpha_M = 3$

Fig. 3. Joint association probability of all cases with different pathloss and different MBS/SBS densities.

becoming shorter, leading to advantage of SBS's signal strength in DL against MBS. In NLOS scenario shown in Fig. 2(b), we can find the similar trend as LOS when joint association probabilities change with SBS/MBS density. An obvious difference is that the probability of Case 4 greatly increases. The main reason is that SBSs have less obstruction and path loss due to shorter range to the vehicles, thereby demonstrating the superiority of SBS in NLOS scenarios. On the whole, decoupling can improve the load balancing of the C-V2X network as the number of SBS increases.

To better understand the characteristics of SBS and MBS, we plot the joint association probabilities against different path loss indices under different SBS/MBS densities, as shown in Fig. 3. Fig. 3(a) and (b) show the association probabilities under different path loss indices α_M of MBS and fixed $\alpha_S = 3$. Fig. 3(c) and (d) show the association probabilities under different path loss indices α_S of SBS and fixed $\alpha_M = 3$. We can see that the probability of Case 2 is decreasing as the link quality of MBS and SBS decreases (i.e., higher values of α) in the four figures of Fig. 3. The joint association probabilities of the three cases are nearly constant since the MBS is not sensitive to the path loss index due to its higher transmit power as shown in Fig. 3(a) and (b). Also, we can see that the probability of Case 4 is increasing in Fig. 3(c) and (d), because the λ_S transformed by the displacement theory decreases as α_S increases. Therefore, after taking the transformed λ_S into the PDF of SBS in (18), the PDF's value at the origin location decreases, the value at the distant point increases, and the overall function increases than before, which means the SBS's path loss index has a greater impact on vehicles close to the SBS, but it increases the association probability to vehicles far away as the α_S increases.

B. Spectral Efficiency

In this section, we plot the SE of each link at first. Then the SE under different joint association cases is plotted and this figure can reflect the SE well while the vehicle is driving on a road.
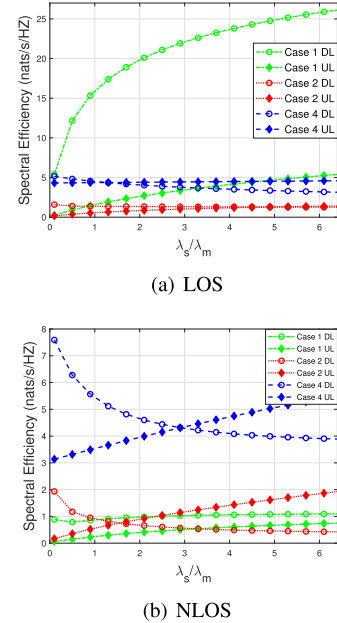

(a) LOS

(b) NLOS

Fig. 4. SE for all decoupled cases in LOS and NLOS scenarios.

The SE of comparison between decoupled access and coupled access is plotted from 0.1 to 6.5 for the ratio of the density of SBS and MBS on the x-axis.

Fig. 4 shows the SE of UL/DL for all cases in LOS and NLOS. We can see that the SE of Case 1's UL and DL are increasing both in LOS and NLOS. The reason is that with the increase of SBS, the closer that the vehicles connected to the MBS, the better the SE of vehicles connected to the MBS is. While in Fig. 4(b), the DL's SE of Case 2, 4 are decreasing because of the increase of SNR as the number of SBS increases.

Fig. 5(a) and (b) show the average SE of three joint association cases in LOS and NLOS scenarios, respectively. And it should be noted that this is not the real link SE obtained by a specific
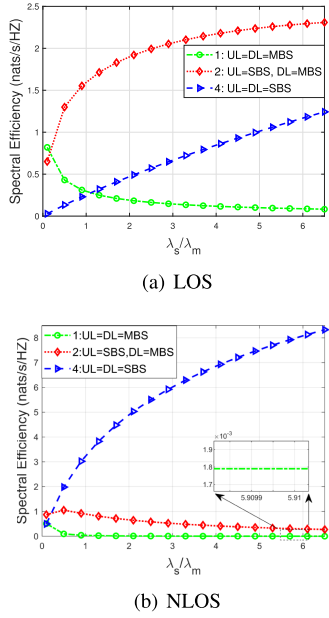
(a) LOS

(b) NLOS

Fig. 5. SE for all decoupled cases in LOS and NLOS scenarios.

(a) LOS

(b) NLOS

Fig. 6. SE for all decoupled and coupled links in LOS and NLOS scenarios.

vehicle, but a weighted average SE like in (39). We can see that the SE of Case 1 is decreasing at the cost of increase of SE of Case 1 as λ_s/λ_m increases both in LOS and NLOS. This is because of the improvement of link quality as there are more SBSs. The SE of Case 2 increases in LOS and decreases in NLOS. The reason is that most vehicles choose Case 2 in LOS and MBS still dominates SBS. While in NLOS, the reason of decreasing in SE of Case 2 is that vehicles originally connected to MBS are connected to SBS instead, resulting in increased interference in DL and the UL's SE doesn't change a lot when a vehicle is connected to MBS.

Fig. 6 shows the SE of UL and DL of decoupled and coupled access in LOS and NLOS scenarios. We can see that the SE is improved in UL after being decoupled over to coupled access, while the DL is the same with the SE of coupled access. Since the DL BS is selected according to the DL reference signal power, the DL of being decoupled is the same as in coupled. While in UL, the vehicles get rid of the limitation of UL/DL coupling through decoupling and can connect to BSs with smaller path loss and shorter distance, so as to improve the UL SE.

For further comparison between decoupled and coupled access, we plot Fig. 7 to show the system average SE by using (39) and the simulation results verify the effectiveness of the theoretical results. The performance improvement shows similar trends as Fig. 6. We can see that the SE of decoupled access is nearly improved by 50% compared with the SE of coupled access in LOS scenario. While in NLOS, the SE advantage of decoupling is not remarkable. The reason is that, in NLOS, most vehicles follow Case 4, as shown in Fig. 2(b), and Case 4 is equivalent to the coupled access case in which the typical vehicle is served by the SBS, the improvement mainly comes from the UL improvement of other cases. And we find that the decoupled mode is more beneficial for networks with higher SBS densities.
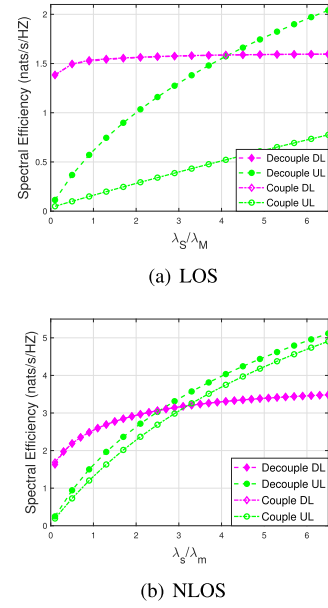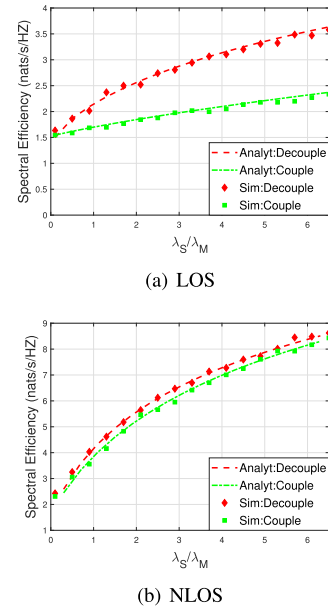

(a) LOS

(b) NLOS

Fig. 7. System average SE for decoupled and coupled cases in LOS and NLOS scenarios.

C. Coverage Probability

Fig. 8 shows the CP of UL/DL for MBS/SBS with different SINR thresholds and different MBS/SBS densities. Obviously, CP decreases with the increase of threshold. It can be found that the CP of both UL and DL of SBS is increasing as λ_S/λ_M increases, while the CP of both UL and DL of MBS is decreasing. The reason is that as there are more SBSs, the distance between vehicles and SBSs becomes closer, thus the association probability of MBS decreases, leading to the decrease in the CP related with MBS (i.e., Case 1, Case 2). The reason for SBS is similar. In a small λ_S/λ_M, we can find that the CP of DL
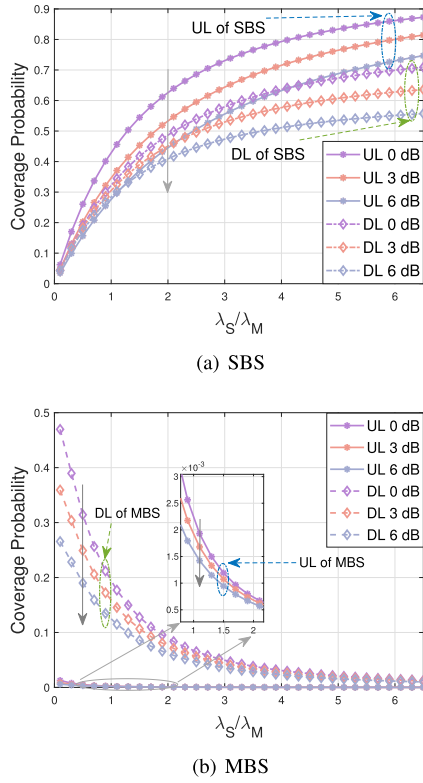
(a) SBS

(b) MBS

Fig. 8. CP for different thresholds ($\lambda_M = 5$ nodes/km^2, $\lambda_l = 1/\pi\ km^{-1}$, and $\lambda_v = 15$ nodes/km).

(a) SBS

(b) MBS
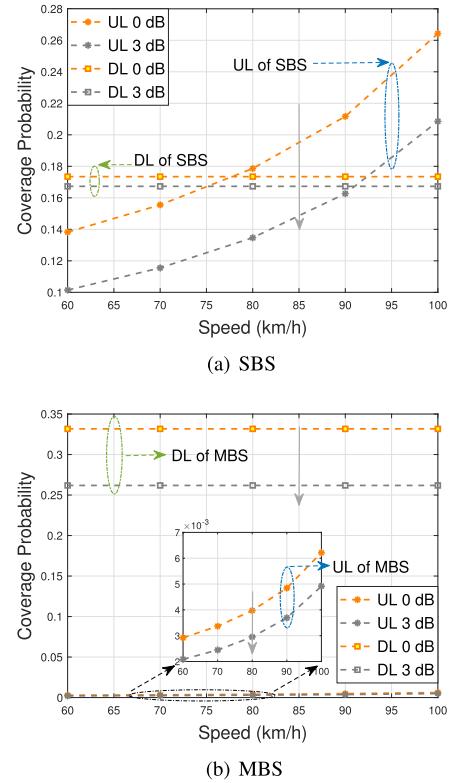
Fig. 9. CP of UL/DL for SBS and MBS as a function of speed ($\lambda_s/\lambda_m = 2/4, \alpha = 4$).

for MBS is much larger than other CPs. This phenomenon also explains the reason why Case 1 and Case 2 are very large as the λ_S/λ_M is small.

D. The Effect of Speed

The vehicle speed influences the vehicle density on the road [45], and the relationship between vehicle speed v and density λ is $v = v_{\max}(1 - \lambda/\lambda_{\max})$ according to the Greenshields Model [46], where $v_{\max}$ and $\lambda_{\max}$ denotes the maximum value of vehicle speed and density, respectively. Thus, we have $\lambda = \lambda_{\max}(1 - v/v_{\max})$. In other words, the speeds of vehicles and the density of vehicles are correlated, which substantially affect the UL CP. According to (22), (26), (31), the speed does not affect the joint association probability. Hence, we plot the CP and SE with different speeds in Figs. 9 and 10, respectively.

In Fig. 9, the CP of UL is increasing, while the CP of the DL remains unchanged as the speed increases for both SBS and MBS. This is because the speed primarily impacts the density of the vehicle, whereas the CP in DL is related with the MBS density and the effect of the vehicle speeds in DL is neglected. According to the relationship between the speed and the vehicle density, a higher speed indicates lower vehicle density. Therefore, the interference in UL is reduced, leading to the increase of CP in UL.

In Fig. 10(a), we can see that the SE of different cases increases as the speed increases. The reason is that the density of vehicles is reduced as the speed increases, thereby reducing
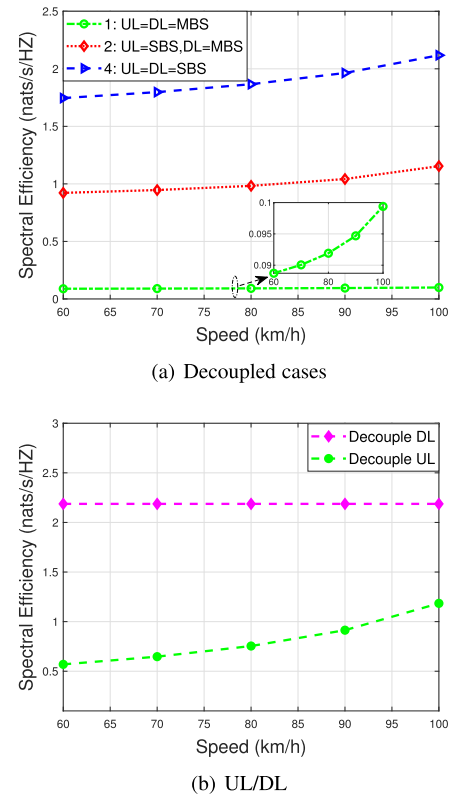

(a) Decoupled cases

(b) UL/DL

Fig. 10. SE for different cases and UL/DL as a function of speed ($\lambda_s/\lambda_m = 2.5/5, \alpha = 4$).

the interference in UL. From Fig. 10(b), we can see that the SE of DL is not affected, while the SE of UL increases as the speed increases. The reason is the same as above. Therefore, the SE gains at different speeds come from UL.

V. CONCLUSION

In this paper, we have done a comprehensive performance analysis of UL/DL decoupled access in C-V2X networks based on stochastic geometry. Specifically, we have modeled the UL/DL decoupled access C-V2X as a Cox process. We have derived the key results that characterize how a vehicle's UL/DL is associated with MBS/SBS from the statistical view, as well as the performance metrics including the joint association probability, the distance distribution of vehicle to BS, the SE, and the CP. With the proposed analytical framework and theoretical results, an in-depth understanding of the decoupled access C-V2X network and its superiority against coupled access have been revealed. The analytical results have been further validated through extensive Monte Carlo simulations. We hope that the work in this paper could promote decoupled access C-V2X network, such that the QoS of various C-V2X applications can be further improved. In future work, we will focus on mobility management and dynamic access optimization in UL/DL decoupled C-V2X networks.

REFERENCES

[1] M. B. Mollah et al., "Blockchain for the Internet of Vehicles towards intelligent transportation systems: A survey," *IEEE Internet Things J.*, vol. 8, no. 6, pp. 4157–4185, Mar. 2021.

[2] Y. Kim et al., "New radio (NR) and its evolution toward 5G-advanced," *IEEE Wirel. Commun.*, vol. 26, no. 3, pp. 2–7, Jun. 2019.

[3] S. Chen, J. Hu, Y. Shi, L. Zhao, and W. Li, "A vision of C-V2X: Technologies, field testing, and challenges with Chinese development," *IEEE Internet Things J.*, vol. 7, no. 5, pp. 3872–3881, May 2020.

[4] J. Zhao et al., "Fully-decoupled radio access networks: A resilient uplink base stations cooperative reception framework," *IEEE Trans. Wireless Commun.*, vol. 22, no. 8, pp. 5096–5110, Aug. 2023.

[5] J. Kang, Z. Xiong, D. Niyato, D. Ye, D. I. Kim, and J. Zhao, "Toward secure blockchain-enabled Internet of Vehicles: Optimizing consensus management using reputation and contract theory," *IEEE Trans. Veh. Technol*, vol. 68, no. 3, pp. 2906–2920, Mar. 2019.

[6] L. Zhang and B. Cao, "Stochastic programming method for offloading in mobile edge computing based Internet of Vehicle," in *Proc. IEEE Int. Conf. Commun.*, 2019, pp. 1–6.

[7] N. Bhushan et al., "Network densification: The dominant theme for wireless evolution into 5G," *IEEE Commun. Mag.*, vol. 52, no. 2, pp. 82–89, Feb. 2014.

[8] F. Boccardi et al., "Why to decouple the uplink and downlink in cellular networks and how to do it," *IEEE Commun. Mag.*, vol. 54, no. 3, pp. 110–117, Mar. 2016.

[9] L. Jiao, K. Yu, Y. Xu, T. Zhang, H. Zhou, and X. Shen, "Spectral efficiency analysis of uplink-downlink decoupled access in C-V2X networks," in *Proc. IEEE Glob. Commun. Conf.*, 2022, pp. 2062–2067.

[10] H. Elshaer, F. Boccardi, M. Dohler, and R. Irmer, "Downlink and uplink decoupling: A disruptive architectural design for 5G networks," in *Proc. IEEE Glob. Commun. Conf.*, 2014, pp. 1798–1803.

[11] L. Yan, X. Fang, and Y. Fang, "A novel network architecture for C/U-plane staggered handover in 5G decoupled heterogeneous railway wireless systems," *IEEE Trans. Intell. Transp. Syst.*, vol. 18, no. 12, pp. 3350–3362, Dec. 2017.

[12] H. Zhou, W. Xu, J. Chen, and W. Wang, "Evolutionary V2X technologies toward the Internet of Vehicles: Challenges and opportunities," *Proc. IEEE*, vol. 108, no. 2, pp. 308–323, Feb. 2020.

[13] J. He, L. Cai, P. Cheng, and J. Pan, "Delay minimization for data dissemination in large-scale VANETs with buses and taxis," *IEEE Trans. Mobile Comput.*, vol. 15, no. 8, pp. 1939–1950, Aug. 2016.

[14] H. S. Dhillon and V. V. Chetlur, "Poisson line cox process: Foundations and applications to vehicular networks," *Synth. Lectures Learn. Netw. Algorithms*, vol. 1, no. 1, pp. 1–149, 2020.

[15] L. Zhang, W. Nie, G. Feng, F.-C. Zheng, and S. Qin, "Uplink performance improvement by decoupling uplink/downlink access in HetNets," *IEEE Trans. Veh. Technol*, vol. 66, no. 8, pp. 6862–6876, Aug. 2017.

[16] R. Li, K. Luo, T. Jiang, and S. Jin, "Uplink spectral efficiency analysis of decoupled access in multiuser MIMO HetNets," *IEEE Trans. Veh. Technol*, vol. 67, no. 5, pp. 4289–4302, May 2018.

[17] K. Smiljkovikj, P. Popovski, and L. Gavrilovska, "Analysis of the decoupled access for downlink and uplink in wireless heterogeneous networks," *IEEE Wireless Commun. Lett.*, vol. 4, no. 2, pp. 173–176, Apr. 2015.

[18] Z. Sattar, J. V. Evangelista, G. Kaddoum, and N. Batani, "Spectral efficiency analysis of the decoupled access for downlink and uplink in two-tier network," *IEEE Trans. Veh. Technol*, vol. 68, no. 5, pp. 4871–4883, May 2019.

[19] Q. Yu et al., "A fully-decoupled RAN architecture for 6G inspired by Neurotransmission," *J. Commun. Inf. Netw.*, vol. 4, no. 4, pp. 15–23, 2019.

[20] Y. Shi, E. Alsusa, and M. W. Baidas, "Energy-efficient decoupled access scheme for cellular-enabled UAV communication systems," *IEEE Syst. J.*, vol. 16, no. 1, pp. 701–712, Mar. 2022.

[21] B. Pan and H. Wu, "Coverage analysis of vehicular safety messages-prioritized C-V2X communications," *IEEE Internet Things J.*, vol. 9, no. 17, pp. 16577–16591, Sep. 2022.

[22] V. V. Chetlur and H. S. Dhillon, "Coverage analysis of a vehicular network modeled as Cox process driven by Poisson line process," *IEEE Trans. Wireless Commun.*, vol. 17, no. 7, pp. 4401–4416, Jul. 2018.

[23] V. V. Chetlur and H. S. Dhillon, "Coverage and rate analysis of downlink cellular vehicle-to-everything (C-V2X) communication," *IEEE Trans. Wireless Commun.*, vol. 19, no. 3, pp. 1738–1753, Mar. 2020.

[24] M. N. Sial, Y. Deng, J. Ahmed, A. Nallanathan, and M. Dohler, "Stochastic geometry modeling of cellular V2X communication over shared channels," *IEEE Trans. Veh. Technol*, vol. 68, no. 12, pp. 11 873–11 887, Dec. 2019.

[25] H.-W. Liu, T.-X. Zheng, Y. Wen, C. Feng, and H.-M. Wang, "Performance analysis of uplink mmwave communications in C-V2X networks," in *Proc. IEEE Glob. Commun. Conf.*, 2020, pp. 1–6.

[26] K. Yu, H. Zhou, Z. Tang, X. Shen, and F. Hou, "Deep reinforcement learning-based RAN slicing for UL/DL decoupled cellular V2X," *IEEE Trans. Wireless Commun.*, vol. 21, no. 5, pp. 3523–3535, May 2022.

[27] V. V. Chetlur, S. Guha, and H. S. Dhillon, "Characterization of V2V coverage in a network of roads modeled as Poisson line process," in *Proc. IEEE Int. Conf. Commun.*, 2018, pp. 1–6.

[28] F. Morlot, "A population model based on a Poisson line tessellation," in *Proc. IEEE 10th Int. Symp. Model. Optim. Mobile Ad Hoc Wirel. Netw.*, 2012, pp. 337–342.

[29] F. Tang, Y. Zhou, and N. Kato, "Deep reinforcement learning for dynamic uplink/downlink resource allocation in high mobility 5G HetNet," *IEEE J. Sel. Areas Commun.*, vol. 38, no. 12, pp. 2773–2782, Dec. 2020.

[30] C. H. Ou, B. Y. Wu, and L. Cai, "GPS-free vehicular localization system using roadside units with directional antennas," *J. Commun. Netw.*, vol. 21, no. 1, pp. 12–24, 2019.

[31] N. C. Beaulieu and C. Cheng, "Efficient Nakagami-m fading channel simulation," *IEEE Trans. Veh. Technol*, vol. 54, no. 2, pp. 413–424, Mar. 2005.

[32] T. Q. Duong, D. B. da Costa, M. Elkashlan, and V. N. Q. Bao, "Cognitive amplify-and-forward relay networks over Nakagami-m fading," *IEEE Trans. Veh. Technol*, vol. 61, no. 5, pp. 2368–2374, Jun. 2012.

[33] H. ElSawy, E. Hossain, and M.-S. Alouini, "Analytical modeling of mode selection and power control for underlay D2D communication in cellular networks," *IEEE Trans. Commun.*, vol. 62, no. 11, pp. 4147–4161, Nov. 2014.

[34] A. Abdulqader Hussein, T. A. Rahman, and C. Y. Leow, "Performance evaluation of localization accuracy for a log-normal shadow fading wireless sensor network under physical barrier attacks," *Sensors*, vol. 15, no. 12, pp. 30 545–30 570, 2015.

[35] Z. Sattar, J. V. Evangelista, G. Kaddoum, and N. Batani, "Analysis of the cell association for decoupled wireless access in a two tier network," in *Proc. IEEE 28th Annu. Int. Symp. Pers. Indoor Mobile Radio Commun.*, 2017, pp. 1–6.

[36] C. Xu, M. Sheng, V. S. Varma, T. Q. Quek, and J. Li, "Wireless service provider selection and bandwidth resource allocation in multi-tier HCNs," *IEEE Trans. Commun.*, vol. 64, no. 12, pp. 5108–5124, Dec. 2016.

[37] P. Madhusudhanan, J. G. Restrepo, Y. Liu, T. X. Brown, and K. R. Baker, "Downlink performance analysis for a generalized shotgun cellular system," *IEEE Trans. Wireless Commun.*, vol. 13, no. 12, pp. 6684–6696, Dec. 2014.

[38] V. V. Chetlur and H. S. Dhillon, "Success probability and area spectral efficiency of a VANET modeled as a Cox process," *IEEE Wireless Commun. Lett.*, vol. 7, no. 5, pp. 856–859, Oct. 2018.

[39] S. N. Chiu, D. Stoyan, W. S. Kendall, and J. Mecke, *Stochastic Geometry and its Applications*. Hoboken, NJ, USA: Wiley, 2013.

[40] J. G. Andrews, F. Baccelli, and R. K. Ganti, "A tractable approach to coverage and rate in cellular networks," *IEEE Trans. Commun.*, vol. 59, no. 11, pp. 3122–3134, Nov. 2011.

[41] M. Haenggi, J. G. Andrews, F. Baccelli, O. Dousse, and M. Franceschetti, "Stochastic geometry and random graphs for the analysis and design of wireless networks," *IEEE J. Sel. Areas Commun.*, vol. 27, no. 7, pp. 1029–1046, Sep. 2009.

[42] M. Matracia, M. A. Kishk, and M.-S. Alouini, "Coverage analysis for UAV-assisted cellular networks in rural areas," *IEEE Open J. Veh. Technol.*, vol. 2, pp. 194–206, 2021.

[43] 3GPP TS 36.885 v14.0.0, "Study on LTE-based V2X services," IEEE Trans. Vehicular Technol., Tech. Rep., Jun. 2016. [Online]. Available: https://portal.3gpp.org/desktopmodules/Specifications/SpecificationDetails.aspx?specificationId=2934

[44] H. Elshaer, M. N. Kulkarni, F. Boccardi, J. G. Andrews, and M. Dohler, "Downlink and uplink cell association with traditional macrocells and millimeter wave small cells," *IEEE Trans. Wireless Commun.*, vol. 15, no. 9, pp. 6244–6258, Sep. 2016.

[45] L. Liang, G. Y. Li, and W. Xu, "Resource allocation for D2D-enabled vehicular communications," *IEEE Trans. Commun.*, vol. 65, no. 7, pp. 3186–3197, Jul. 2017.

[46] B. D. Greenshields, J. Bibbins, W. Channing, and H. Miller, "A study of traffic capacity," *Highway Res. Board Proc.*, vol. 14, no. 1, pp. 448–477, 1935.

Tingting Liu (Member, IEEE) received the BS degree in communication engineering and the PhD degree in information and communication engineering from Nanjing University of Science and Technology, Nanjing China, in 2005 and 2011, respectively. From 2017 to 2018, she was a visiting scholar with the University of Houston, Houston, TX, USA. She is currently a full professor with Nanjing University of Posts and Telecommunications, Nanjing, Jiangsu, China. Her research interests include game theory, Internet of vehicles, blockchain, caching-enabled systems, edge computing, network quality of service, device-to-device networks, and cognitive radio networks.

Haibo Zhou (Senior Member, IEEE) received the PhD degree in information and communication engineering from Shanghai Jiao Tong University, Shanghai, China, in 2014. From 2014 to 2017, he was a postdoctoral fellow with the Broadband Communications Research Group, Department of Electrical and Computer Engineering, University of Waterloo. He is currently a full professor with the School of Electronic Science and Engineering, Nanjing University, Nanjing, China. He was elected as an IET fellow, in 2022, highly cited researcher by Clarivate Analytics, in 2022 & 2020. He was a recipient of the 2019 IEEE ComSoc Asia.Pacific Outstanding Young Researcher Award, 2023–2024 IEEE ComSoc Distinguished Lecturer, and 2023–2025 IEEE VTS Distinguished lecturer. He served as Track/Symposium co-chair for IEEE/CIC ICCC 2019, IEEE VTC-Fall 2020, IEEE VTC-Fall 2021, WCSP 2022, IEEE GLOBECOM 2022, IEEE ICC 2024. He is currently an associate editor of the *IEEE Transactions on Wireless Communications*, *IEEE Internet of Things Journal*, *IEEE Network Magazine*, and *Journal of Communications and Information Networks*. His research interests include resource management and protocol design in B5G/6G networks, vehicular ad hoc networks, and space-air-ground integrated networks.

Luofang Jiao (Member, IEEE) received the BS degree in detection guidance and control technology from the University of Electronic Science and Technology of China, Chengdu, China, in 2020. He is currently working toward the PhD degree with the School of Electronic Science and Engineering, Nanjing University, Nanjing, China. His research interests include uplink/downlink decoupled access, C-V2X, and heterogeneous networks.

Kai Yu (Member, IEEE) received the BS degree in detection guidance and control technology from the University of Electronic Science and Technology of China, Chengdu, China, in 2019. He is currently working toward the PhD degree with the School of Electronic Science and Engineering, Nanjing University, Nanjing, China. His research interests include resource allocation, machine learning for wireless communications, and heterogeneous networks.

Jiacheng Chen (Member, IEEE) received the PhD degree in information and communications engineering from Shanghai Jiao Tong University, Shanghai, China, in 2018. From 2015 to 2016, he was a visiting scholar with the BBCR Group, University of Waterloo, Waterloo, ON, Canada. He is currently an assistant researcher with Peng Cheng Laboratory, Shenzhen, China. His research interests include future network design, 5G/6G network, and resource management.

Lin Cai (Fellow, IEEE) received the MASc and PhD degrees (awarded Outstanding Achievement in Graduate Studies) in electrical and computer engineering from the University of Waterloo, Waterloo, ON, Canada, in 2002 and 2005, respectively. Since 2005, she has been with the Department of Electrical and Computer Engineering, University of Victoria, Victoria, BC, Canada, where she is currently a professor. Her research interests span several areas in communications and networking, with a focus on network protocol and architecture design supporting emerging multimedia traffic and the Internet of Things. She was a recipient of the NSERC Discovery Accelerator Supplement Grants in 2010 and 2015, respectively, and the Best Paper Awards of IEEE ICC 2008 and IEEE WCNC 2011. She has co-founded and chaired the IEEE Victoria Section Vehicular Technology and Communications Joint Societies Chapter. She has been elected to serve the IEEE Vehicular Technology Society Board of Governors from 2019 to 2021. She has served as an area editor for *IEEE Transactions on Vehicular Technology*, a member of the Steering Committee of *IEEE Transactions on Big Data* and *IEEE Transactions on Cloud Computing*, an associate editor of *IEEE Internet of Things Journal*, *IEEE Transactions on Wireless Communications*, *IEEE Transactions on Vehicular Technology*, *IEEE Transactions on Communications*, *EURASIP Journal on Wireless Communications and Networking*, *International Journal of Sensor Networks*, and *Journal of Communications and Networks*, and as the distinguished lecturer of IEEE VTS Society. She has served as the TPC co-chair for IEEE VTC2020-Fall, and the TPC Symposium co-chair for IEEE Globecom'10 and Globecom'13. She is a Registered professional engineer in British Columbia, Canada. She is an NSERC E.W.R. Steacie Memorial fellow.